COMPDYN 2011
3rd ECCOMAS Thematic Conference on
Computational Methods in Structural Dynamics and Earthquake Engineering
M. Papadrakakis, M. Fragiadakis, V. Plevris (eds.)
Corfu, Greece, 25–28 May 2011

QUASI-STATIC SIMULATIONS OF THIN SPACE MEMBRANES, AIMING AT STABILITY ANALYSES OF BALLOON-LIKE STRUCTURES

Anders Eriksson

KTH Mechanics, Royal Institute of Technology
Osquars backe 18, SE-100 44 Stockholm, Sweden
e-mail: anderi@kth.se

Keywords: Space membranes, Inflation, Compressible medium, Quasi-static equilibrium, Stability, Path-following.

Abstract. *This paper discusses the evaluation of quasi-static equilibrium solutions for inflatable space membrane structures, such as balloons. A flat linearly interpolated triangular element is used for simulations, with a Mooney-Rivlin hyper-elastic material model, with variable constitutive constants. A compressible medium is used to introduce a one-parametric over-pressure loading within the membrane. Complex path-following procedures are used to find generalized equilibrium paths, with different parameterizations. Numerical examples show that the methods developed can give information on the stability of the structures, but that the medium and means for introducing the internal pressure is of importance for the interpretation of stability.*

1 INTRODUCTION

A large variety of thin three dimensional inflatable structures, i.e., balloons, are used in several engineering and medical contexts, e.g., [1, 2, 3]. These structures often show large deformations when subjected to distributed pressures. The bending stiffness can often be neglected and only a membrane state considered. Several analytical and numerical treatments for more or less general situations are available in literature, [4, 5, 6, 7, 8]. The treatment of these structures also leads to several accompanying aspects, such as the load descriptions, [9], contact formulations, [10], and instability aspects, [11, 12, 13].

Simulations of very thin membranes are often based on shell models, but these show important drawbacks in situations where the bending stiffness almost vanishes. The main problems lie in the treatment of large rotations, the aspect ratios of the elements, and the stiffness differences in membrane and bending action. As one remedy, rotation-free shell elements have been suggested by many researchers, [14, 15, 16, and others]. The main efforts have been related to non-local evaluation of the element curvatures, and to degenerated solid elements, [17]. Advantages and disadvantages of rotation-free shell elements are described in [18, 19].

For the balloon-like structures considered in the present work, an assumption has been that simulations of the inflation process can be based purely on the membrane behavior, disregarding the bending stiffness. This assumption will remove the numerical problems associated with shell formulations when thickness tends to zero, and also leads to efficient simulations. Some space membrane elements have been developed in literature for special applications. An interesting recent development is discussed by Pargana et al., [20], where an initially flat, quadratically interpolated 6-node membrane element is developed for 'Tensioned Fabric' structures. The element uses a total Lagrangian approach, and Green strains, but considers only cases where strains can be assumed as small.

The problems considered here, i.e., the inflation of balloon-like structures, are both geometrically non-linear due to finite deformations and materially non-linear through the constitutive relationship. A co-rotational ('CR') finite element form was developed in [21], where the local element is purely in an in-plane state. It was concluded that the CR formulation can be relevant and efficient for problems where the local behavior is sufficiently well described by an elastic formulation, but that the formulation became inefficient when hyper-elastic material models were introduced. In the present work, a hyper-elastic flat triangular membrane element based on a total Lagrangian ('TL') formulation was used for the analysis of thin space membrane structures, allowing different hyper-elastic forms.

The restrictions of the current formulation are primarily that all elements connecting to a node can not be co-planar at any stage, and that only surface-normal pressure loads are present. For physical relevance, the elements in the mesh must also be under tensile states at any solution. We also only consider quasi-static equilibrium situations, hypothesizing that he dynamics of a real inflation process is not primarily related to the inertia properties of the structure, but to the loading situations. The quasi-static assumption in this work means that any combination of pressure and volume can be immediately introduced, without dynamic or thermal effects.

The element formulation was tested for the structural class considered, noting that the present problems demand sophisticated path-following algorithms, with several aspects of instability detection and classification included. In particular, the generalized path-following in a parameter space with not just a single load factor was shown to be useful for the analyses.

2 COMPUTATIONAL MODELING

The basic quasi-static structural equilibrium situation is based on a one-parametric pressure loading. The formulation is thereby aimed at seeking a set of combinations $(\boldsymbol{u}, \psi)$ satisfying:

$$\boldsymbol{F}(\boldsymbol{u}, \psi) \equiv \boldsymbol{f}(\boldsymbol{u}) - \boldsymbol{p}(\psi, \boldsymbol{u}) = \boldsymbol{0} \tag{1}$$

where $\boldsymbol{f}$, $\boldsymbol{p}$, and $\boldsymbol{u}$ are vectors containing internal forces, external forces, and displacements, respectively, in the degrees of freedom of the structure considered. Also, ψ is a scalar value representing the over-pressure in the transversal direction. Element displacements $\boldsymbol{u}^g$ are extracted from $\boldsymbol{u}$ based on a topology defined, while $\boldsymbol{f}$ and $\boldsymbol{p}$ are assembled from element contributions $\boldsymbol{f}^g$ and $\boldsymbol{p}^g$, respectively. The super-index g indicates that the element components are measured in the common degrees of freedom of the structure, which in the present case are translations in the three global axis directions.

The differential relation corresponding to Eq. (1) is:

$$\delta \boldsymbol{F} = \frac{\partial \boldsymbol{f}}{\partial \boldsymbol{u}} \delta \boldsymbol{u} - \frac{\partial \boldsymbol{p}}{\partial \boldsymbol{u}} \delta \boldsymbol{u} - \frac{\partial \boldsymbol{p}}{\partial \psi} \delta \psi = (\mathbf{K} - \mathbf{K}_p)\, \delta \boldsymbol{u} - \delta \psi \frac{\partial \boldsymbol{p}}{\partial \psi} \tag{2}$$

which gives a tangential stiffness matrix containing a load-dependent term, since the pressure load is acting on the deformed geometry.

2.1 Element formulation

The element used for large deflection space membrane simulations is based on the linearly interpolated constant strain triangle, 'CST', for in-plane analysis. When seen in a three-dimensional context, the nodes (i, j, k) are defined by initial coordinates $\boldsymbol{x}_I^g,\ (I = i, j, k)$. The global displacement components are similarly $\boldsymbol{u}_I^g$. The element is assumed to be flat, and the initial nodal positions define a plane in space, with three initial element coordinate axes in an orthogonal matrix $\mathbf{R}_0$, the third axis being an outwards normal direction to the flat element. Using the initial position of node i as the origin for a local coordinate system, the initial shape of the element is defined by local coordinates:

$$\boldsymbol{x}_I^e = \mathbf{R}_0^T\, (\boldsymbol{x}_I^g - \boldsymbol{x}_i^g) \qquad (I = i, j, k) \tag{3}$$

where the third coordinate is zero for the three nodes, by construction. Relative to this initial element coordinate system, the displacements are:

$$\boldsymbol{u}_I^e = \mathbf{R}_0^T\, \boldsymbol{u}_I^g \qquad (I = i, j, k) \tag{4}$$

The displacements of a point p within the element is interpolated as:

$$\boldsymbol{u}_p^e = \sum_I N_I(x_{p,1}^e, x_{p,2}^e) \boldsymbol{u}_I^e \tag{5}$$

with common shape functions for the CST element, representing a linear interpolation of all three local displacement components related to the initial element plane.

Corresponding to the element displacements $\boldsymbol{u}_I^e$, element internal forces $\boldsymbol{f}_I^e$ are evaluated, which are then transformed into internal force contributions in global coordinate directions as:

$$\boldsymbol{f}_I^g = \mathbf{R}_0\, \boldsymbol{f}_I^e \qquad (I = i, j, k) \tag{6}$$

The evaluation of the internal forces in the element is assuming an incompressible isotropic hyper-elastic material model. Strains are described by the the right Cauchy-Green deformation tensor:

$$\mathbf{C} = \begin{bmatrix} C_{11} & C_{12} & 0 \\ C_{21} & C_{22} & 0 \\ 0 & 0 & C_{33} \end{bmatrix} \tag{7}$$

where the incompressibility condition $J = \det(\mathbf{C}) = 1$ relates C_{33} to the other components, and where initial element coordinates are used. Stresses are represented by the second Piola-Kirchhoff stress tensor:

$$\mathbf{S} = \begin{bmatrix} S_{11} & S_{12} & 0 \\ S_{21} & S_{22} & 0 \\ 0 & 0 & S_{33} \end{bmatrix} \tag{8}$$

where the assumption of a local plane-stress situation demands $S_{33} = 0$.

Introducing the constraints above, a convenient form can be derived based on considering the four components C_{11}, C_{22}, C_{12} and C_{21}, and the corresponding stress components. It is noted that the strains are non-linearly dependent on nodal displacements but constant over the element area. An incremental strain operator $\mathbf{B} = \mathbf{B}(\boldsymbol{x}_I^e, \boldsymbol{u}_I^e)$ gives variations in strain components from variations in element displacements.

The hyper-elastic model is characterized by a strain-energy relation, [22, 23]:

$$\mathbf{S} = -\rho\,\mathbf{C}^{-1} + 2\frac{\partial W}{\partial \mathbf{C}} \tag{9}$$

where W is a strain energy function, and ρ a hydro-static pressure, which can also be seen as a Lagrange multiplier enforcing the strain and stress constraints above. With the incompressibility assumption, $I_3(\mathbf{C}) = 1$, the strain energy function is written:

$$W = W(I_1(\mathbf{C}), I_2(\mathbf{C})) \tag{10}$$

with the first and second invariants of the tensor $\mathbf{C}$. A Mooney-Rivlin form, [22] defines the stress-strain relation from two constitutive constants:

$$W = c_1(I_1(\mathbf{C}) - 3) + c_2(I_2(\mathbf{C}) - 3) \tag{11}$$

The above expressions were used to describe the relation between the stress and strain components considered:

$$\mathbf{S} = \mathbf{S}(\mathbf{C}, c_1, c_2) \tag{12}$$

and also the differential relation between increments in stress and strain. These give the internal force vector and the tangential stiffness matrix for the element at a current state of displacement; as all quantities are constant within each element, the required integration is simple.

A neo-Hookean form is a further specialization of the above expression, where a single constitutive constant is $c_1 = \mu/2$, half the shear modulus. A general demand on the constants is that the sum $c_1 + c_2 = \mu/2$, [22]. Different relations between the two constitutive constants were tested for the numerical examples below, and are in the examples represented as a ratio n_1/n_2, where:

$$c_1 = \frac{n_1}{n_1 + n_2}\frac{\mu}{2} \tag{13}$$

$$c_2 = \frac{n_2}{n_1 + n_2}\frac{\mu}{2} \tag{14}$$

2.2 Loading assumptions

A membrane can be pressurized in several different ways. One important aspect is the medium introducing the pressure on the membrane. Typically, a gas is compressible and can be assumed to have zero density, whereas a liquid is incompressible and has a density. In particular for gases, the mechanism for introducing the medium into the membrane is of importance, where it is assumed that either a specified pressure can be introduced independent of the resulting volume, or a specific amount of gas is introduced leading to a balance between pressure and volume.

In the present work, it has been assumed that the pressure is introduced by a compressible gas, with zero density. This means that a one-parameter description of the over-pressure can be used, and this pressure is acting in a normal, outwards direction on all surfaces, with only positive over-pressures considered. The over-pressure ψ is seen as related to a constant surrounding pressure of the membrane ψ_0. The total pressure within the membrane is thereby $\Psi = \psi_0 + \psi$.

The local displacement-dependent loading due to normal uniform over-pressure is evaluated as:

$$\boldsymbol{p}_I^e = \psi \frac{A}{3} (0, 0, 1)^{\mathrm{T}}, \quad (I = i, j, k) \tag{15}$$

where ψ is the current surface pressure, and $A = A(\boldsymbol{x}_I^e, \boldsymbol{u}_I^e)$ is the current element area. The element contribution is transformed to global degrees of freedom and assembled to the structural pressure load vector.

The stiffness term $\mathbf{K}_p$ in Eq. (2) is related to the displacement-dependent pressure loads. This aspect is extensively discussed in [11], and must be considered when simulating large deformations of a pressure-loaded structure. Assembled from element contributions $\mathbf{K}_p^g$, rather simple geometric consideration show that for the present formulation:

$$\mathbf{K}_p^g = \mathbf{R}_0 \begin{bmatrix} \mathbf{k}_{p,ii} & \mathbf{k}_{p,ij} & \mathbf{k}_{p,ik} \\ \mathbf{k}_{p,ji} & \mathbf{k}_{p,jj} & \mathbf{k}_{p,jk} \\ \mathbf{k}_{p,ki} & \mathbf{k}_{p,kj} & \mathbf{k}_{p,kk} \end{bmatrix} \mathbf{R}_0^{\mathrm{T}} \tag{16}$$

where the submatrices are formulated in displaced local coordinates:

$$\mathbf{k}_{p,IJ} = \frac{\psi}{6} \begin{bmatrix} 0 & 0 & y_{d(J-1)} - y_{d(J+1)} \\ 0 & 0 & x_{d(J+1)} - x_{d(J-1)} \\ y_{d(J+1)} - y_{d(J-1)} & x_{d(J-1)} - x_{d(J+1)} & 0 \end{bmatrix} \tag{17}$$

The indices i, j, k are thereby introduced cyclically, and the coordinates are

$$\boldsymbol{x}_{dI} = \begin{pmatrix} x_{dI} \\ y_{dI} \\ z_{dI} \end{pmatrix} = \boldsymbol{x}_I^e + \boldsymbol{u}_I^e \tag{18}$$

The amount of gas contained by the membrane can be evaluated from the equation for an ideal gas, stated as:

$$\Psi V = NT \tag{19}$$

where Ψ is the total gas pressure, V the volume enclosed by the membrane, N an amount measure and T the absolute temperature. This expression can be used in different ways in the evaluation of membrane behavior, as indicated by the examples below.

2.3 Quasi-static equilibrium solutions

The pressurized membranes often show complicated non-linear responses to loading, with different instability states being important aspects. The solution of quasi-static equilibrium states thereby demands rather sophisticated solution algorithms. The present work has utilized one-dimensional path-following techniques based on variable parameterizations along the solution path, changing both the parameterizing component and the step length as functions of the path traversed, [24, 25]. The isolation of critical instability states is based on sequential bisections along the parameterized path, [26]. The response variables can also be seen as functions of, e.g., geometric or material parameters in the model, [27], where augmenting equations specify a subset of equilibrium states under variation of the additional parameters. In particular, the dependence of the critical states on the added parameters can be evaluated by methods from [28]. An interesting possibility, not yet utilized, is also to to evaluate two-dimensional solution surfaces, where parametric combinations leading to certain response aspects can be evaluated and visualized, [29]. The general setting is thereby:

$$\boldsymbol{G}(\boldsymbol{u},\boldsymbol{\lambda}) \equiv \begin{pmatrix} \boldsymbol{f}(\boldsymbol{u}) - \boldsymbol{p}(\lambda_1,\boldsymbol{u}) \\ \boldsymbol{g}(\boldsymbol{u},\boldsymbol{\lambda}) \end{pmatrix} = \boldsymbol{0} \tag{20}$$

where Eq. (1) gives the equilibrium equations between the displacements and the load-describing variable $\lambda_1 = \psi$, and the N_g augmenting equations $\boldsymbol{g}(\boldsymbol{u},\boldsymbol{\lambda})$ define some extra relations for the interesting subset of equilibrium solutions, under the variations of the variables $\lambda_1,\ldots,\lambda_{N_\lambda}$. The dimension of the solutions to the augmented system is then $N_\lambda - N_g$.

3 NUMERICAL EXAMPLES

We have performed some test with a spherical membrane, and a balloon-shaped membrane, both subjected to internal over-pressures. In both cases, we used an initial thickness of 0.1 mm, and a material with shear modulus $\mu = 0.4225$ MPa.

3.1 A sphere

A sphere with radius $r = 10$ mm under internal pressure was considered, [4, 22]. Boundary conditions were chosen to allow uniform expansion, cf Fig. 1. A mesh of the whole sphere with 5120 triangular elements was considered, based on successive subdivisions of a 20-corner icosahedron mesh; all nodes were moved radially to be placed on the sphere. The example was used to show the properties of the hyper-elastic formulation, with different ratios between c_1 and c_2 coefficients in the Mooney-Rivlin constitutive relation Eq. (11), described by (n_1, n_2) as in Eqs. (13)–(14).

The results from hyper-elastic models are given in Fig. 2. Re-drawn with the radial expansion u_D expressed as a stretch, the results visually agree with the analytical results given in [22], for $c_1 = 0.5\mu, c_2 = 0$ ('neo-Hookean') and for $c_1 = \frac{7}{16}\mu, c_2 = \frac{1}{16}\mu$ ('Mooney-Rivlin'). No instabilities were noted in addition to the turning points with respect to pressure, [4].

Solutions with a sufficiently low c_2 constant show a maximum pressure state for small expansions. Even for very small non-zero values of c_2, there will also be a (local) minimum pressure state, but the pressures will eventually increase with radial expansion; this was verified for a case with $(n_1/n_2) = 1023/1$, where the minimum limit pressure was found as $p = 0.528$ kPa at a radial expansion $u_D \approx 310$ mm. The pair of limit pressure states disappear between calculated solutions for $n_1/n_2 = 5/1$ and $n_1/n_2 = 4/1$.

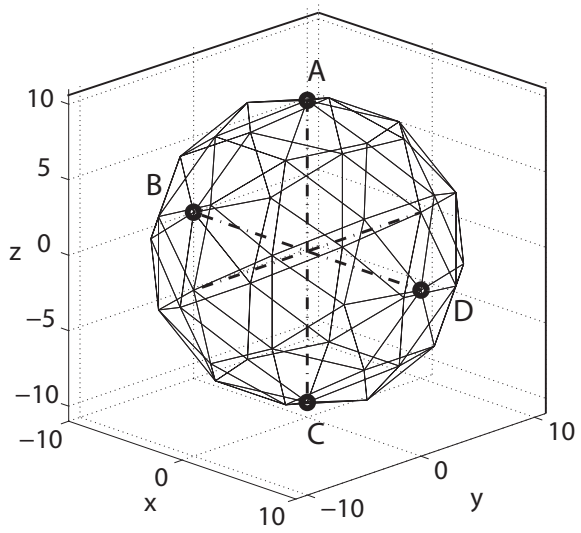

Figure 1: Sphere under internal pressure. The figures shows an eighty element model, and sample points, but calculations were performed with an 5120 element mesh. Supports were given as: $u_A = v_A = v_B = u_C = v_C = w_C = 0$, with (u, v, w) the translations in global (x, y, z) directions.

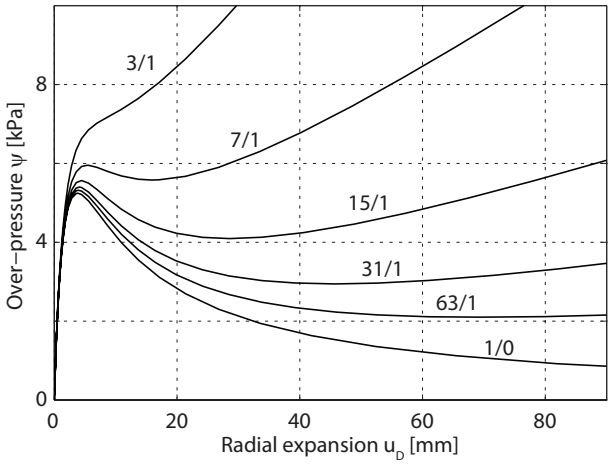

Figure 2: Sphere under internal pressure. Radial expansion and internal over-pressure for different parameters in a Mooney-Rivlin model. Curve notation n_1/n_2 according to Eqs. (13)–(14).

3.2 A long balloon

Figure 3 shows a model with 672 triangular elements of an inflated balloon which is completely fixed in one end, $x = 0$, constrained to only axial movement of the farthest end (A), and subjected to a uniform internal pressure ψ, assuming a surrounding pressure of $\psi_0 = 100\,\text{kPa}$. The initial geometry of the balloon was composed of a $L = 95\,\text{mm}$ cylinder with radius $r = 10\,\text{mm}$ and an end half-sphere. Sample points for deflections are marked in Fig. 3. Quasi-static equilibrium simulations were performed for refined models with 2688 and 10752 elements.

The pressure-expansion sequence was followed by a displacement-based iteration sequence for a 10752 element mesh, and different hyper-elastic material model, described by the ratio n_1/n_2 in Eqs. (13)–(14). The result is represented by the radial expansion v_D related to the internal over-pressure ψ in Fig. 4. A set of longitudinal sections through the inflated balloon are shown in Fig. 5. The profiles show the section of the balloon at $z = 0$, but the section $y = 0$

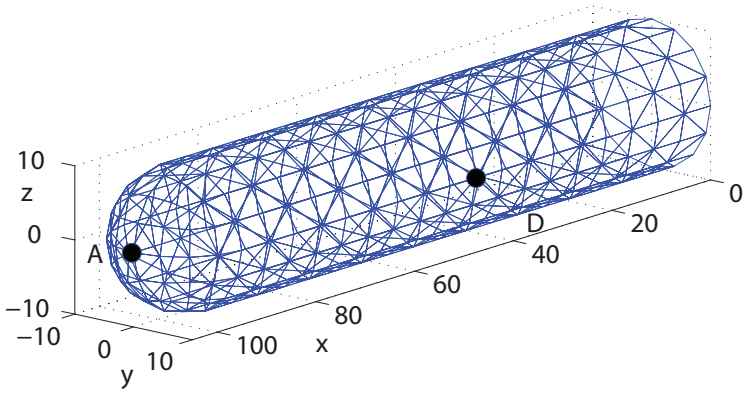

Figure 3: Inflation of balloon, 672 element model with sample points. All nodes at $x = 0$ were considered fully fixed in the simulations, the node at A could only move axially; all other nodes were completely free. Calculations were made with refined models (2688, 10752 elements), obtained from successive divisions of the figure elements into four triangles.

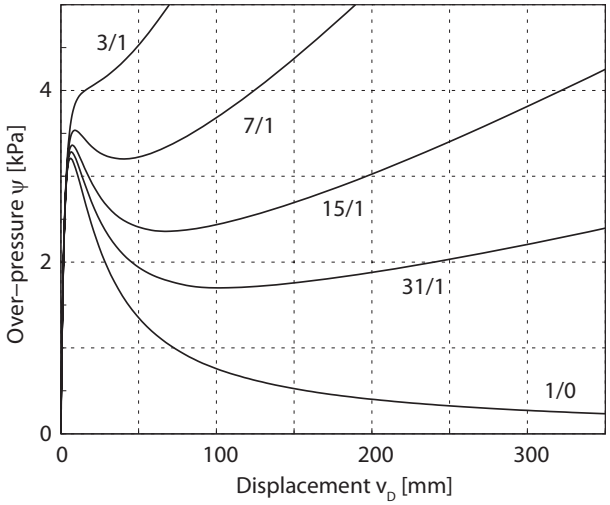

Figure 4: Inflation of balloon. Hyper-elastic material models, and 10752 element mesh. Quasi-static equilibrium paths, represented by internal over-pressure ψ and radial expansion at sample point D, v_D, Fig. 3. Curve notation n_1/n_2 according to Eqs. (13)–(14).

gives completely identical figures, as all solutions are rotationally symmetric. The sections were chosen when the radial expansion $v_D \approx 300\,\text{mm}$ for the different material models; the position of sample point D is marked by a circle in the figures. It is noted that these solutions refer to significantly different pressures ψ, cf. Fig. 4.

The dots on the sections in Fig. 5 show the displaced positions of the nodes on the symmetry line, which were close to evenly distributed initially. It is obvious that the neo-Hookean model $n_1/n_2 = 1/0$ will give a considerably different behavior than the other models, as it localizes the strains to the central parts of the balloon. This is an effect of the softening behavior with strain, whereas a non-zero c_2 coefficient will give a final stiffening of the material. This localization of the straining means that the mesh must be finer for the neo-Hookean material, in order to avoid behavior artifacts from the discretization. The 2688 element model was shown to be essentially free from such artifacts even for the neo-Hookean case.

Several of the material models showed a limit state with respect to internal over-pressure: a maximum load point, which was isolated to high accuracy. This limit state existed for all tested

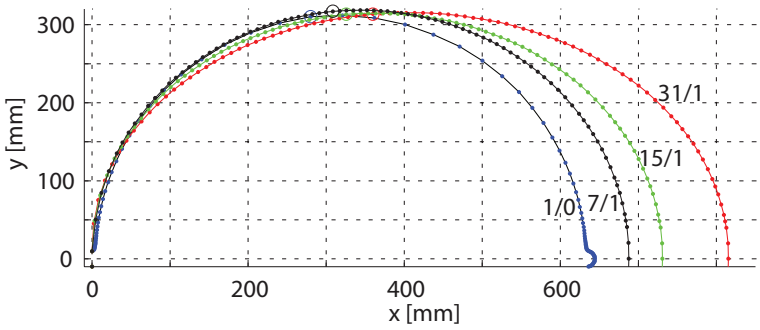

Figure 5: Inflation of balloon. Hyper-elastic material models, and 10752 element mesh. Sections through inflated balloon, for solutions with $v_D \approx 300\,\text{mm}$, for different parameters in a Mooney-Rivlin model. Curve notation n_1/n_2 according to Eqs. (13)–(14).

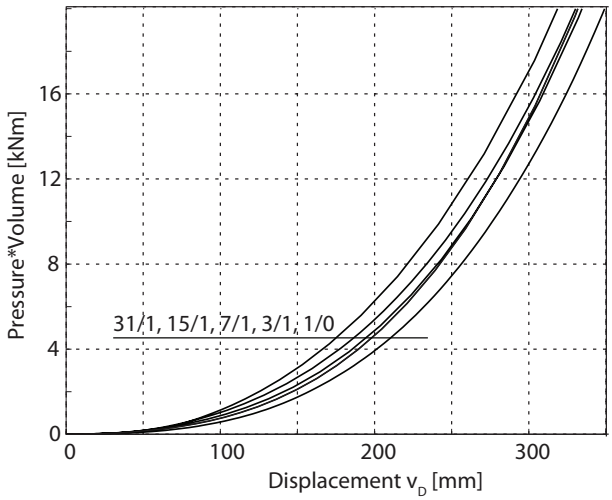

Figure 6: Inflation of balloon. Hyper-elastic material models, and 10752 element mesh. Radial expansion v_D related to the amount of gas injected, represented by product $(\psi_0+\psi)V(\boldsymbol{u})$, for different parameters in a Mooney-Rivlin model. Curve notation n_1/n_2 according to Eqs. (13)–(14). Surrounding pressure $\psi_0 = 100\,\text{kPa}$.

material models with ratios $n_1/n_2 \geq 5$, whereas no (local) maximum pressure state was found for $n_1/n_2 \leq 4$. Except for the neo-Hookean model, the maximum pressure state corresponded to a (local) minimum before the pressure started to increase monotonically with expansion. A loading situation where the pressure can be regulated would thus show a dynamic snap-through behavior in the inflation process for such materials.

The models showed bifurcation states for very large expansions. For the $n_1/n_2 = 7/1$ model with 10752 elements, this occurred at an overpressure $\psi = 43.9\,\text{kPa}$, and a radial expansion $v_D = 2139\,\text{mm}$ with a mode corresponding to a torsion of the balloon. The same bifurcation was found for $\psi = 59.0\,\text{kPa}$, $v_D = 1435\,\text{mm}$ when $n_1/n_2 = 3/1$. It is noted that some possible instability modes are restrained by the adopted kinematic constraints.

The results in Fig. 4 are represented as radial expansion v_D and product $(\psi_0 + \psi)V(\boldsymbol{u})$ in Fig. 6, for the assumed $\psi_0 = 100\,\text{kPa}$, and the volume V calculated from the current displacements $\boldsymbol{u}$. For all material models, the expansion is monotonically increasing together with the injected amount of gas, so no instability would occur in the process for a loading situation where the inflow of gas is regulated. It is noted, however, that the evaluation of the injected amount of gas is significantly dependent on the assumed surrounding pressure.

As an alternative to the above solution, the solution of the inflation problem can also be

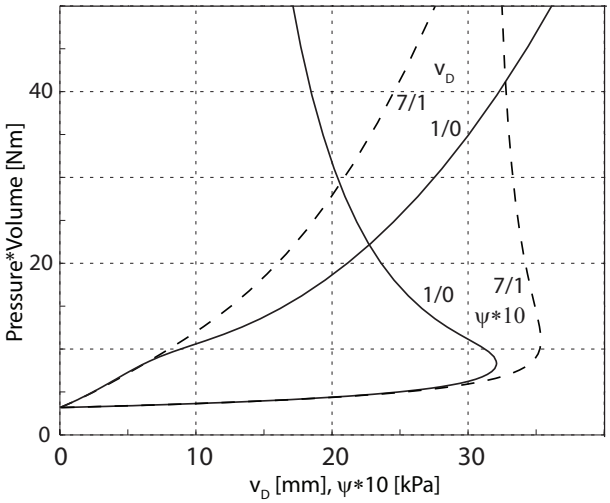

Figure 7: Inflation of balloon. Hyper-elastic material models, and 2688 element mesh. Solutions parameterized by amount measure, for different parameters in a Mooney-Rivlin model. Radial expansion v_D and internal over-pressure ψ, Fig. 3. Curve notation n_1/n_2 according to Eqs. (13)–(14). Surrounding pressure $\psi_0 = 100\,\text{kPa}$.

parameterized by the amount of gas injected. Assuming isothermal conditions, a second control variable $\lambda_2 = N_t$ was used in addition to the over-pressure $\lambda_1 = \psi$, together with an augmenting equation:

$$g(\boldsymbol{u}, \boldsymbol{\lambda}) = (\psi_0 + \lambda_1)V(\boldsymbol{u}) - \lambda_2 = 0 \tag{21}$$

Driving the path-following with the λ_2 variable gave the results presented in Fig. 7, for different constitutive parameters c_1, c_2. The solutions are identical to the ones obtained without the amount parameter.

The augmenting equation method was used to study the behavior of an inflated balloon under change of temperature. The problem was set up with three control variables $\boldsymbol{\lambda}^{\mathrm{T}} = (\psi, N, T)$, with two augmenting equations beside the equilibrium equations:

$$\boldsymbol{g}(\boldsymbol{u}, \boldsymbol{\lambda}) = \begin{pmatrix} (\psi_0 + \lambda_1)V(\boldsymbol{u}) - \lambda_2\,(\lambda_3 + 273) \\ \lambda_2 - N_0 \end{pmatrix} = \boldsymbol{0} \tag{22}$$

where N_0 is a constant, defined in each material model case from the primary solutions in Fig. 4 for an over-pressure of $\psi = 3.0\,\text{kPa}$, and assuming that this situation was first achieved at $T = 20°\text{C}$, whereafter the balloon was sealed. The solutions obtained for variable temperature are shown in Fig. 8

4 CONCLUDING REMARKS

In this paper, a faceted triangular membrane space element is used for the analysis of pressurized membrane structures, using a class of hyper-elastic, Mooney-Rivlin, material models. The loading was seen as a uniform over-pressure, representing a gas loading. Quasi-static conditions were assumed, neglecting dynamic effects primarily coming from the flow velocities within the volume. It is emphasized by examples that the pressurizing mechanism is of importance for the response, even when the analysis is restricted to gas as the pressurizing medium. Two simple 'balloon-type' membranes show that limit points can occur when the pressure variable is seen as the parameter for the inflation, whereas these limit states can disappear when the injected gas

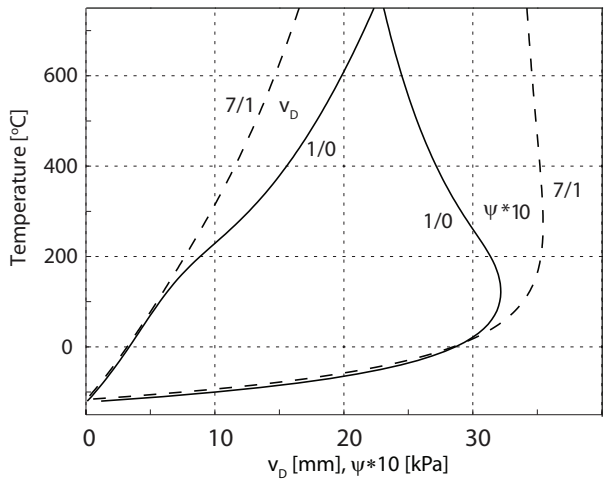

Figure 8: Inflation of balloon. Hyper-elastic material models, and 2688 element mesh. Solutions parameterized by temperature, for different parameters in a Mooney-Rivlin model. Radial expansion v_D and internal over-pressure ψ, Fig. 3. Curve notation n_1/n_2 according to Eqs. (13)–(14). Surrounding pressure $\psi_0 = 100\,\text{kPa}$.

volume is seen as the parameter. This difference thus has significance for the dynamic response of the membrane.

The results from the numerical examples indicate that the proposed formulation can be used for analysis of space membrane problems showing large displacements and large strains. The present study has been limited to uniform internal over-pressures, but other media or methods for introduction of the pressure, as well as partially filled structures, are interesting continuations of the project reported. A requirement for the model to be useful in the analysis of realistic structures is the development and verification of other non-linear material models.

A sophisticated path-following algorithm is needed for following the complex generalized equilibrium paths, which are used for the simulations. It is believed that the two-dimensional equilibrium surfaces discussed in [29] can be used for an improved understanding of membrane behavior under different classes of loadings.

REFERENCES

[1] J. A. Main, S. W. Peterson, A. M. Strauss, Load-deflection behavior of space-based inflatable fabric beams, J. Aerospace Eng. 7 (2) (1994) 225–238.

[2] D. K. Liang, D. Z. Yang, M. Qi, W. Q. Wang, Finite element analysis of the implantation of a balloon-expandable stent in a stenosed artery, Int. J. cardiol. 104 (3) (2005) 314–318.

[3] B. Bénech, A. Ezcurra, M. Lothon, F. Saïd, B. Campistron, F. Lohou, P. Durand, Constant volume balloons measurements in the urban Marseille and Fos-Berre industrial ozone plumes during ESCOMPTE experiment, Atm. Env. 42 (22) (2008) 5589–5601.

[4] A. Needleman, Inflation of spherical rubber balloons, Int. J. Solids Struct. 13 (5) (1977) 409–421.

[5] P. D. Gosling, W. J. Lewis, Optimal structural membranes — I. Formulation of a curved quadrilateral element for surface definition, Comput. Struct. 61 (5) (1996) 871–883.

[6] D. T. Berry, H. T. Y. Yang, Formulation and experimental verification of a pneumatic finite element, Int. J. Numer. Meth. Eng. 39 (7) (1996) 1097–1114.

[7] J. Bonet, R. D. Wood, J. Mahaney, P. Heywood, Finite element analysis of air supported membrane structures, Comput. Methods Appl. Mech. Engrg. 190 (5-7) (2000) 579–595.

[8] F. Cirak, M. Ortiz, Fully C^1-conforming subdivision elements for finite deformation thin-shell analysis, Int. J. Numer. Meth. Eng. 51 (7) (2001) 813–833.

[9] K. Schweizerhof, E. Ramm, Displacement dependent pressure loads in nonlinear finite element analyses, Comput. Struct. 18 (6) (1984) 1099–1114.

[10] D. E. Kiousis, T. C. Gasser, G. A. Holzapfel, Smooth contact strategies with emphasis on the modeling of balloon angioplasty with stenting, Int. J. Numer. Meth. Eng. 75 (7) (2008) 826–855.

[11] T. Rumpel, K. Schweizerhof, Volume-dependent pressure loading and its influence on the stability of structures, Int. J. Numer. Meth. Eng. 56 (2) (2003) 211–238.

[12] A. N. Gent, Elastic instabilities in rubber, Int. J. Numer. Meth. Eng. 40 (2-3) (2005) 165–175.

[13] L. M. Kanner, C. O. Horgan, Elastic instabilities for strain-stiffening rubber-like spherical and cylindrical thin shells under inflation, Int. J. Non-lin. Mech. 42 (2) (2007) 204–215.

[14] R. Phaal, C. R. Calladine, Simple class of finite elements for plate and shell problems. II: An element for thin shells, with only translational degrees of freedom, Int. J. Numer. Meth. Eng. 35 (5) (1992) 979–996.

[15] J. K. Hampshire, B. H. V. Topping, H. C. Chan, Three node triangular bending elements with one degree of freedom per node, Eng. Comput. 9 (1) (1992) 49–62.

[16] E. Oñate, M. Cervera, Derivation of thin plate bending elements with one degree of freedom per node: a simple three node triangle, Eng. Comput. 10 (6) (1993) 543–561.

[17] R. Hauptmann, K. Schweizerhof, A systematic development of 'solid-shell' element formulations for linear and non-linear analyses employing only displacement degrees of freedom, Int. J. Numer. Meth. Eng. 42 (1) (1998) 49–69.

[18] E. Oñate, F. Zárate, Rotation-free triangular plate and shell elements, Int. J. Numer. Meth. Eng. 47 (1-3) (2000) 557–603.

[19] M. Gärdsback, G. Tibert, A comparison of rotation-free triangular shell elements for unstructured meshes, Comput. Methods Appl. Mech. Engrg. 196 (49-52) (2007) 5001–5015.

[20] J. B. Pargana, D. Lloyd-Smith, B. A. Izzuddin, Fully integrated design and analysis of tensioned fabric structures: Finite elements and case studies, Eng. Struct.(doi: 10.1016/j.engstruct.2009.12.032).

[21] A. Eriksson, S. Farughi, Quasi-static inflation simulations based on a co-rotational triangular space membrane element, Int. J. Struct. Stab. Dyn.(submitted).

[22] G. A. Holzapfel, Nonlinear solid mechanics. A continuum approach for engineering, Wiley, Chichester, 2000.

[23] C. Truesdell, The elements of continuum mechanics, Springer, Berlin, 1966.

[24] A. Eriksson, On linear constraints for Newton-Raphson corrections and critical point searches in structural F. E. problems, Int. J. Numer. Meth. Eng. 28 (1989) 1317–1334.

[25] A. Eriksson, R. Kouhia, On step size adjustments in structural continuation problems, Comput. Struct. 55 (1995) 495–506.

[26] A. Eriksson, Equilibrium subsets for multi-parametric structural analysis, Comput. Methods Appl. Mech. Engrg. 140 (1997) 305–327.

[27] A. Eriksson, Structural instability analyses based on generalised path-following, Comput. Methods Appl. Mech. Engrg. 156 (1998) 45–74.

[28] A. Eriksson, Fold lines for sensitivity analyses in structural instability, Comput. Methods Appl. Mech. Engrg. 114 (1994) 77–101.

[29] A. Eriksson, C. Pacoste, Solution surfaces and generalised paths in non-linear structural mechanics, Int. J. Struct. Stab. Dyn. 1 (2001) 1–30.